https://doi.org/10.1016/j.buildenv.2022.109487

Airborne transmission of exhaled pollutants during short-term events: quantitatively assessing inhalation monitor points

Xiujie Li [a], Cheuk Ming Mak [a]*, Zhengtao Ai [b, c], Hai Ming Wong [d]

a Department of Building Environment and Energy Engineering, The Hong Kong Polytechnic University, Hong Kong, China

b Department of Civil Engineering, Hunan University, Changsha, China

c National Center for International Research Collaboration in Building Safety and Environment, Hunan University, Changsha, China

d Faculty of Dentistry, The University of Hong Kong, Hong Kong, China

*Corresponding author. Email address: cheuk-ming.mak@polyu.edu.hk

Abstract:

The infection risk assessment associated with the contaminant inhalation can provide a scientific basis for formulating mitigation measures. Previous studies on the breathing zone are primarily based on the assumption of the steady formation and homogeneous property, while it might not be applicable for short-term events. Large-eddy simulation (LES) is employed in the present study, as well as two computational thermal manikins with detailed facial features and transient breathing conditions. Exposure risks in eight commonly used monitor points are compared in short-term events and under steady-state conditions. Three representative physical distances between room occupants are investigated, namely 0.35 m, 1.0 m, and 1.5 m. Based on the statistical difference in the contaminant distribution at a short physical distance, the breathing zone could be identified from the time-averaged concentration field. The results highlight that the previously defined breathing zone ignores unsteady airflow characteristics, significantly impacting the exposure risk estimation in short-term events. Owing to the substantial temporal variation of the contaminant in the identified breathing zone, the instant exposure risk analysis in short-term events should consider its turbulence intensity and concentration fluctuation characteristic. Overall, instead of using the identified breathing zone. Point_A, Point_B, and Point_C should be employed to evaluate infection risk in short-term events. The localized method with direct interference on the respiratory airflow should be recommended in short-term events.

Keywords: Airborne transmission; LES turbulence model; Short-term events; Breathing zone; Exposure risk.

1. Introduction

The COVID-19 pandemic rising from the severe acute respiratory syndrome coronavirus (SARS-CoV-2) has ravaged the world since 2020. According to the WHO weekly report, as of April 3rd, 489 million and 6.1 million get infection and death, respectively [1]. The economic development and the provision of medical measures have been severely affected [2]. Recently, much more attention has been attracted to the human infection risk analysis associated with contaminant inhalation and the breathing zone [3-5]. The virus-laden aerosols and droplets generated during human respiratory activities (like breathing, speaking, and coughing) could be the potential transmission routes [6, 7]. The small particles could remain suspended in the air for prolonged periods and may be inhaled into the susceptible human respiratory tract [8]. Several precautionary measures have been proposed to prevent and control cross-transmission, like keeping social distance, wearing surgical masks, and frequent hand washing. To provide evidence for the social distancing, plenty of numerical [9-12] and experimental studies [13-15] have been conducted to investigate the transmission of exhaled viruses. Liu et al. numerically evaluated the effect of social distances on the cross-transmission risk and found the threshold distance of 1.0 - 1.5 m for short-range and long-range airborne routes [16]. During the COVID-19 crisis, the social distance of 1.5 m has been widely adopted [17]. However, some studies pointed out that environmental factors like humidity and ventilation could affect the transmission distance [18-20]. Given that airborne transmission is relatively more complicated in mechanisms and mitigation measures, the understanding of the airborne transmission routes of SARS-CoV-2 is far from sufficient.

Traditionally, the “breathing zone” is vaguely defined as the region near the human’s mouth and nose (the radius is around 15 cm) [21]. However, applying the detailed breathing zone in practice seems difficult in the human exposure risk assessment due to the strong airflow interaction in a multi-person interior environment. Besides, considering the uneven distribution of virus-laden particles in the breathing zone, simply treating it as a whole zone may under-/over-estimate the contaminant inhaled by the susceptible subjects. How to select appropriate monitor points in different scenarios is still not well investigated, especially when the inhaled contaminant cannot be measured. The employment of only one monitor point within the proposed breathing zone is still common. For example, Al Assaad D et al. [22] evaluated the contaminant concentration in the breathing zone by sampling at 0.15 m below the mouth, as the thermal plume could carry the contaminant to the breathing zone. Otmar Geiss [23] measured the carbon dioxide (CO_2) concentration in the breathing zone when wearing face masks, and the sampling point was just above the nose tip on the bridge of the nose. Donghyun Rim et al. [24] recorded the inhaled virus concentration by the sampling point in front of the mouth at a distance of 0.05 m. Kierat et al. [5] experimentally evaluated the performance of the sampler locations and the sampling methods but only focused on the scenario of one person. Whereas the airflow collision in a multi-person interior environment could further affect the contaminant distribution. In addition, many previous studies did not point out the unequivocal location of the sampling point [25-27]. Recently, Kuga et al. [4] quantitatively studied the breathing zone based on the assumption of its steady formation. However, in practice, the formation of the breathing zone should be treated as unsteady, especially for short-term events [28]. Overall, the aforementioned simplifications about the steady formation and homogenous property in the breathing zone could lead to the discrepancy in human exposure risk assessment.

With the development of computational resources, numerical simulations have been extensively employed to investigate pollutant transmission and airflow patterns. However, there still are some simplifications on the computational thermal manikins, like the complex geometry, transient breathing cycle, and body movement. Although it has been recognized that facial features can affect the flow field and the contaminant distribution [29-31], plenty of numerical simulations have been conducted without considering the facial effect owing to the model complexity and extensive computational resources [32, 33]. Anthony et al. [29] experimentally found that the facial features could affect the flow field (20 mm) near the mannequin's face, but without considering the thermal plume. Also, Li et al. [30] numerically investigated the breathing airflow velocity and proved that the facial features could result in the non-uniform velocity profiles at the nostril openings. More recently, Yan et al. [31] evaluated the effect of the manikin simplification on the thermal plume and pointed out that the surface smoothed model (without facial features) could induce considerable global error on the contaminant transport. Besides, the simplified breathing cycle only with "steady inhalation" could not reproduce the real situation. It may overestimate the scope of the breathing zone [34-36]. The aforementioned simplifications on the facial features and the transient breathing cycle could considerably affect the contaminant distribution and further impact the simulation accuracy. As a result, future computational fluid dynamic (CFD) simulations should consider the complex geometry of the human body and the transient breathing cycle, including both inhalation and exhalation.

Numerous short-term exposure events have been reported in public spaces, especially during the ongoing COVID-19 pandemic. The cross-transmission induced by the Delta variant of SARS-CoV-2 is reported to occur in tens of seconds [37, 38]. The clustered outbreaks highlight the importance of evaluating the instant exposure risks of susceptible subjects. However, many previous studies are limited in the contaminant transmission under steady-state conditions. The two-equation Reynolds-averaged

Navier-Stokes (RANs) turbulence models are extensively employed in different scenarios, like hospital rooms [39, 40], vehicles [41], and even different building floors [42, 43]. The short-term events in the present study refer to the building-up background concentration, which indicates the infected subject has just entered the space. Considering the turbulent nature of the human thermal plume and the breathing airflow, the fluctuation characteristics of the airflow could significantly affect the contaminant distribution in the breathing zone. Besides, the characteristics of airborne transmission in short-term events and under steady-state conditions are considerably distinctive [15]. Ai et al. [28] experimentally found that the instant exposure risk in short-term events constantly varies over time. The instant exposure risk might not always increase with time. Considering the low-resolution characteristics of the aforementioned experimental study, it is necessary to explore the fluctuation of instant exposure risk in short-term events by the CFD analysis. Hence, the formation of the breathing zone and instant exposure risk assessment associated with the contaminant inhalation should be properly evaluated, especially for short-term events. Given that the Direct Numerical Simulation (DNS) requires significant computer resources, the Large Eddy Simulation (LES) is more suitable for evaluating the instantaneous contaminant distribution in turbulent airflow.

The objective of the present study is to analyze the breathing zone characteristics in short-term events and under steady-state conditions. The LES turbulence model is employed to predict the airborne transmission, and two computational thermal manikins with detailed facial features and transient breathing conditions are considered. The breathing zone would be identified from the time-averaged concentration field by comparing the monitor points and inhalation. In addition, the predicted exposure risk in short-term events, steady-state conditions, and three representative distances would then be investigated. The inhalation monitor points in the identified breathing zone would be compared under different conditions. The obtained results of the present study could help to select the proper monitor points and develop mitigation measures for short-term events.

2. Methods

2.1 Model description

As presented in Fig. 1, the computational domain is constructed to represent the office room with the dimension of 4.7 m length x 4.4 m width x 2.7 m height. Two computational thermal manikins (CTMs) are placed in the central plane of the room and kept with the face-to-face posture. The three representative physical distances of 0.35 m, 1.0 m, and 1.5 m between two CTMs are examined. The CTM A and B represent the infected and susceptible subjects, respectively. The breathing model of the two CTMs is assumed to be mouth exhalation and nose inhalation for the infected subject and mouth inhalation and nose exhalation for the susceptible one. The breathing model is synchronized in the simulation, and the aforementioned breathing combination is considered the most prone to cross-infection [35]. The pulmonary ventilation rate is defined as 6.0 L/min, with respiratory rates ten times/min [44]. The geometry of the

CTM presented in Fig. 2 indicates the average-size woman with detailed facial features. Mixing ventilation is adopted in the office room, with the air supply and exhaust in the middle and corner of the ceiling. Besides, the room is in 6 air changes per hour (ACH) and maintained at 24 ℃ to meet the thermal comfort of the human body. The domain is large enough that the surrounding room walls will not impact the flow field near the human body. The previous experimental studies focusing on short-term events were conducted in a full-scale test room with three ventilation types. Two breathing thermal manikins were placed in the chamber with different standing positions and physical distances. The tracer gas concentration was monitored by the instruments, including a Fast Concentration Meter and an INNOVA Multi-gas Sampler and Monitor, to evaluate the transient exposure indexes. The experimental study examined the dynamic characteristics of short-term events, and a detailed description of the apparatus and experimental procedures could be found in the previous article [28].

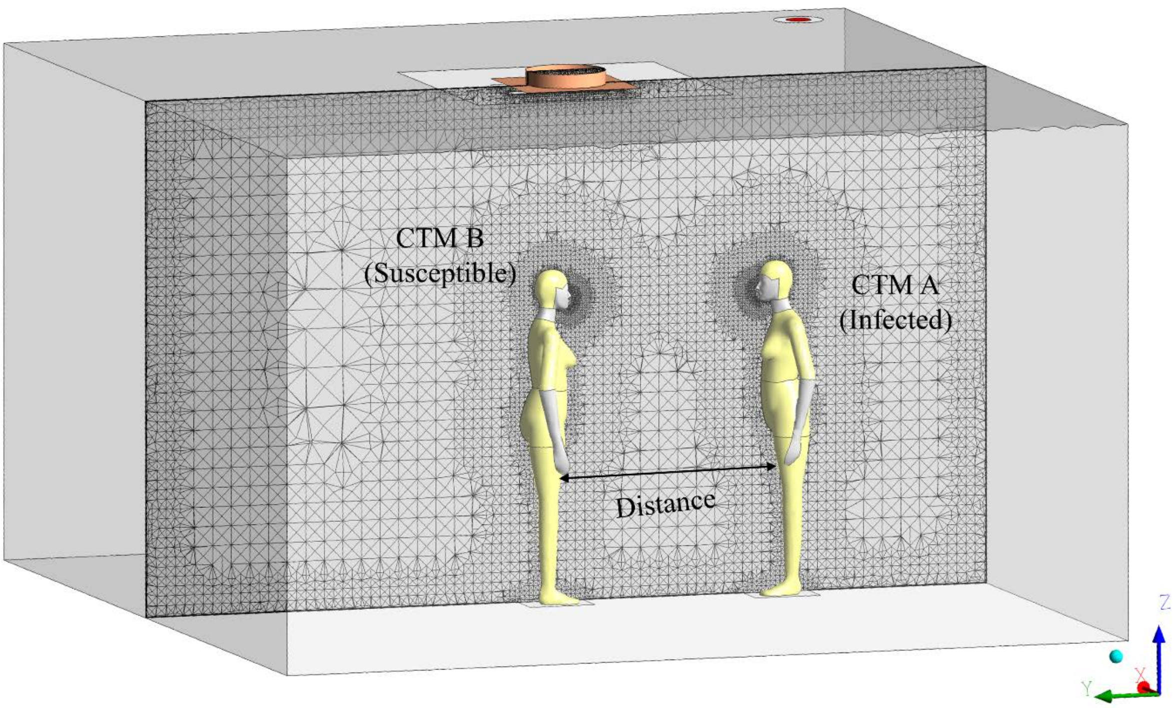

Fig. 1 The computational domain representing two computational thermal manikins (CTMs) in the office room with mixing ventilation.

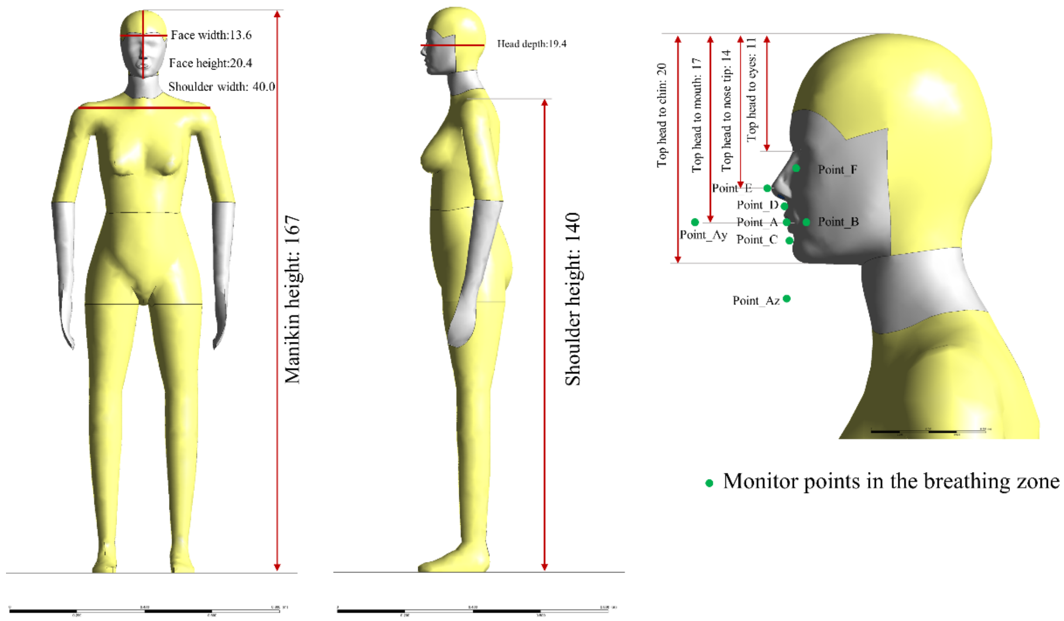

Fig. 2 the CTM employed in this study with detailed facial features (units: cm) and the monitor points in the breathing zone.

Owing to the difficulty of applying the detailed breathing zone to evaluate exposure risk in practice, eight widely-used monitor points are placed near the mouth and nose of CTMs (detailed location data in Table 1). The monitor points are selected based on previous studies [4, 5, 22, 23, 45]. In addition to comparing contaminant concentrations, the turbulence intensity and concentration fluctuation characteristics are also compared in short-term events and under steady-state conditions.

Table 1 The location of the monitor points in the breathing zone of the susceptible subject.

Location	Description
Point_A	At the center of the lips
Point_Az	At 0.15 m below the mouth [22]
Point_Ay	At 0.15 m ahead of the mouth (left limit of traditional breathing zone)
Point_B	At the left corner of the mouth [4]
Point_C	At the center between the chin and lower lip [5]
Point_D	At the center between the upper lip and nose [5]
Point_E	At the nose tip [23, 45]
Point_F	Close to the left eye (upper limit of traditional breathing zone)

2.2 Boundary condition

The ventilation supply diffuser is set as the velocity inlet (0.74 m/s), keeping the temperature (23 ℃). The ventilation exhaust is specified as a pressure outlet with zero-gauge pressure. The exhaust air temperature was set as 26 ℃. The room wall is adiabatic. The total heat power of each CTM is set as 80 W, where the proportion of convective heat load is defined as 30%. Thus, a convective heat load of 24 W is employed for the CTM, and the radiation is not considered in the present study. The cross-sectional area of each nostril and mouth is 38.5 mm^2 and 158 mm^2, respectively [46]. The angle of the jet's airflow from the nostrils is 45 degrees with the horizontal plane and 30 degrees between the two jets [47]. The airflow direction from the mouth is roughly horizontal. The breathing combination of the CTMs is assumed to be mouth exhalation and nose inhalation for the infected subject and mouth inhalation and nose exhalation for the susceptible one. Besides, the periodical sinusoidal breathing is composed of 2.5 s inhalation, 2.5 s exhalation, and 1.0 s break [48, 49]. Given the dynamic breathing boundary conditions of the CTMs, the User-defined function (UDF) is employed to set the transient velocity profiles, with a constant outlet temperature of 34 ℃. The function of the mouth and nose exhalation velocities against time is the sine function, expressed as $V = 0.378 * sin\,(1.26t),\ 2.5\,s < t < 5.0\,s,$ where $V\ is$ the volume flow rate, $L/s. t$ is time, s. The turbulence intensity of the exhaled airflow is defined as 5%. The mass fraction of the N_2O in the infected subject's exhalation airflow is assigned as 0.027, which is in line with that of CO_2 in the human exhalation airflow [50].

Owing to the complex geometry of the human body and face, the unstructured grid with tetrahedral-shaped elements is employed. A refinement of 0.8 mm is adopted for the mouth and nostrils to capture the airflow collision and contaminant distribution. The maximum cell size of the face is limited to 10 times that of the mouth and nostrils [50], and the maximum cell size of the body is maintained at four times the maximum cell size of the face. The results present around 80,000 triangles on the CTMs' surface. To provide better resolution of the airflow profiles in the boundary layer, five layers of the prismatic cells are generated, and the dimensionless wall distance y+ is ensured to be less than 1.

The 'PISO' algorithm is employed to solve the flow field, owing to its performance in transient scenarios. The second-order upwind scheme discretizes all equations. The transient formulation is resolved by the second-order implicit method. The performance of different sub-grid scale models has been evaluated by Bazdidi-Tehrani et al. [51]. A slight difference (5%) between the wall-adapting local eddy-viscosity (WALE) model and the standard Smagorinsky-Lilly model (SSLM) is found in predicting the time-averaged concentration field and concentration fluctuation. In addition, the SSLM has also been widely employed to study the flow pattern and contaminant transmission in indoor and outdoor environments [52-54]. Therefore, airflow is simulated using the LES turbulence model with the SSLM. Since the time step of 0.02 s for high–velocity coughing and talking has shared similar results as 0.001 s [55], the time step of 0.04 s for transient respiration is employed in the present study. The employed time step could ensure that the model captured the smallest chronological changes in the flow field without increasing computing costs. Since the present study focused on short-term events under the building-up background concentration, the steady-state condition refers to when the averaged airspeed and contaminant concentration in the ventilation exhaust reaches relatively stable [28]. Considering the large-eddy turnover time has been employed as the convergence criteria [35], both the large-eddy turnover time and the stability of ventilation exhaust are combined to determine the solution convergence in the present study. The solution convergence is treated to be satisfied when reaching five eddy turnover times, and the residuals can reach 10^{-5} among cases in different physical distances. The large-eddy turnover time is the characteristic timescale defined as the largest scale of the computational domain (w) divided by the friction velocity

(v_0) [35]. In this study, the $w = 4.7\,m$, and estimated v_0 could be obtained by dividing the ventilation airflow rate by a half section of the domain.

2.3 Statistical method

To better understand the contaminant distribution in the breathing zone for short-term events and steady-state conditions, the phase-averaged exposure index $\varepsilon_p(t)$ is employed to reveal the concentration variations. The phase-averaged exposure index $\varepsilon_p(t)$ is calculated from the arithmetic mean of concentration in the monitor points during the inhalation phase. The exposure risk index has been extensively employed to indicate the relationship between ventilation and infection risk [56, 57]. Since the aforementioned risk assessment model is limited to the steady-state condition, the improved method proposed by Ai et al. [28] is adopted to evaluate the infection risk of the susceptible subjects in short-term events (Eq. (1)).

$$\overline{\varepsilon_p(t)} = \frac{\overline{C_{\mathrm{in}}(t)}}{\overline{C_{exhaust-steady}}} \tag{1}$$

where, $\overline{C_{\mathrm{in}}(t)}$ refers to the arithmetic mean of concentration in the monitor points during the inhalation phase. $\overline{C_{exhaust-steady}}$ means the arithmetic mean of concentration in ventilation exhaust after a short-term exposure event has developed to the steady-state. The improved method could consider the high volatility characteristics of the inhaled contaminant.

Further analysis of the turbulence intensity (TI) and its concentration fluctuation characteristic could provide substantial insight into the breathing zone. The time-averaged TI (Eq. (2)) and phase-averaged TI (Eq. (3)) are also employed to indicate the fluctuation characteristics of velocities, as follows:

$$TI = u_n'/\overline{u_n} \tag{2}$$

$$TI_{phase} = u_{\mathrm{in}}'/\overline{u_{\mathrm{in}}} \tag{3}$$

where the u_n' refers to the standard deviation of the velocity in the monitor point n; $\overline{u_n}$ is the mean velocity. u_{in}' and $\overline{u_{\mathrm{in}}}$ refer to the standard deviation and arithmetic mean of the velocity in the monitor points during the inhalation phase, respectively.

3 Results and discussion

3.1 Validation study

To verify the accuracy of the LES turbulence model, the velocity distribution around the standing manikin is employed to make the comparison. The particle image velocimetry (PIV) experiment conducted by Licina et al. [58] aimed to investigate the human convective boundary layer in a quiescent environment. Compared with a hot-wire anemometer, the PIV, without interfering with the flow field, has been widely used to visualize the flow and measure the instantaneous velocity [59]. The maximum mean velocity distribution at each height was measured close to the surface of the standing manikin. The vertical velocity profile in the fifteen monitor points recorded in the case of the standing manikin is employed to validate the numerical simulation. In Fig. 3 (a), the continuous velocity profile of 61 s- 65 s in the LES turbulence model is averaged. In addition, the RNG $k-\varepsilon$ model is also employed by keeping the same settings as the LES turbulence model. The velocity magnitude counter at 65 s is extracted to provide the supplementary figure of the LES turbulence model (in Fig. 3 (b)). Several local high-velocity regions are successfully captured in the CFD simulation, such as in front of the face and chest. Besides, the lower velocity at the height of the chin is accurately depicted, which is attributed to the head behaving like a physical obstacle. Four statistical metrics are selected to quantify the accuracy of the LES turbulence model [60], namely the correlation coefficient (R), the fraction bias (FB), the normalized mean square error $(NMSE)$, and the fraction of predictions within a factor of two of observation $(FAC2)$. In this study, the four statistical performance metrics are all within the recommended criteria: $R = 0.973\,(> 0.8)$, $|FB| = 0.0015\,(< 0.3)$, $NMSE = 0.011\,(< 4)$, $FAC2 = 1\,(> 0.5)$. In comparison with the LES turbulence model, the unsteady RANS approach just models the turbulence and resolves only unsteady mean flow structures [61]. Since the present study focuses on short-term events, the contaminant fluctuation depends not only on the turbulence intensity near the facial region but could also be affected by the turbulent energy distribution among the eddies of different sizes. Therefore, it is critical to employ the LES turbulence model to resolve the eddies of the turbulence itself.

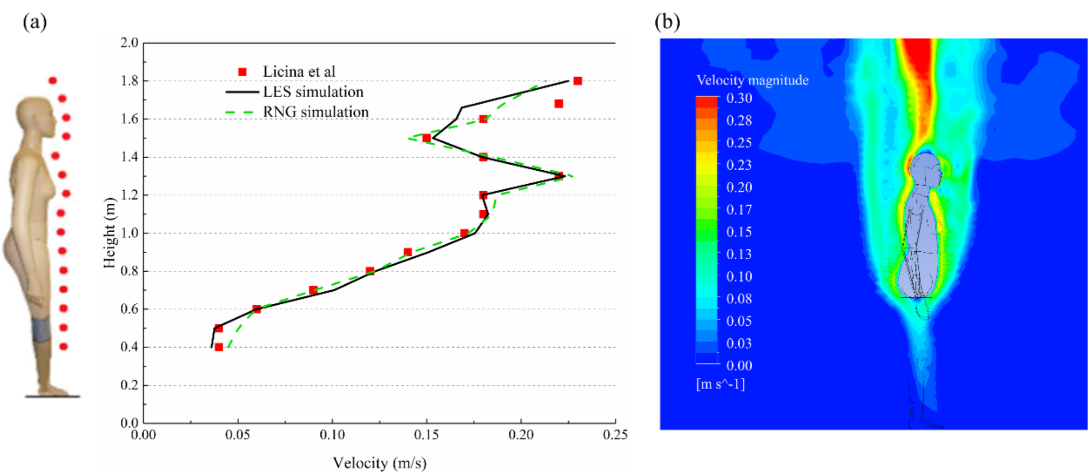

Fig.3 Vertical velocity profile around CTM versus PIV experiment: a) velocity distribution with height; b) velocity magnitude counter at the moment of 65 s.

3.2 Flow field and contaminant distribution

The velocity distribution and airflow interaction between room occupants are presented in Fig. 4, along with the time in different rows (61.5 s, 63.0 s, 64.5 s, and 66.0 s) for three representative physical distances (0.35 m, 1.0 m, and 1.5 m). The absence of phase difference between the two breathing models means 61.5 s representing that both room occupants are in the inhalation phase. The 63.0 s and 64.5 s refer to the different moments of the exhalation process, and 66.0 s is the break between breaths. Similar to the previous study [62], the exhalation airflow is relatively stable initially, with a mushroom shape, as shown in the 63 s in the figure. As the exhalation airflow develops (in Fig. 4, the 64.5 s), it gradually becomes chaotic, and a vortex appears on top of the airflow. In comparison with the other two distances, strong airflow interaction is observed at the physical distance of 0.35 m. Although the thermal plume can prevent the penetration of contaminants, the high-momentum airflow exhaled from the infected subject's mouth still directly reaches the facial region of the susceptible one. Minor differences in the velocity distribution are found between the physical distances of 1.0 m and 1.5 m.

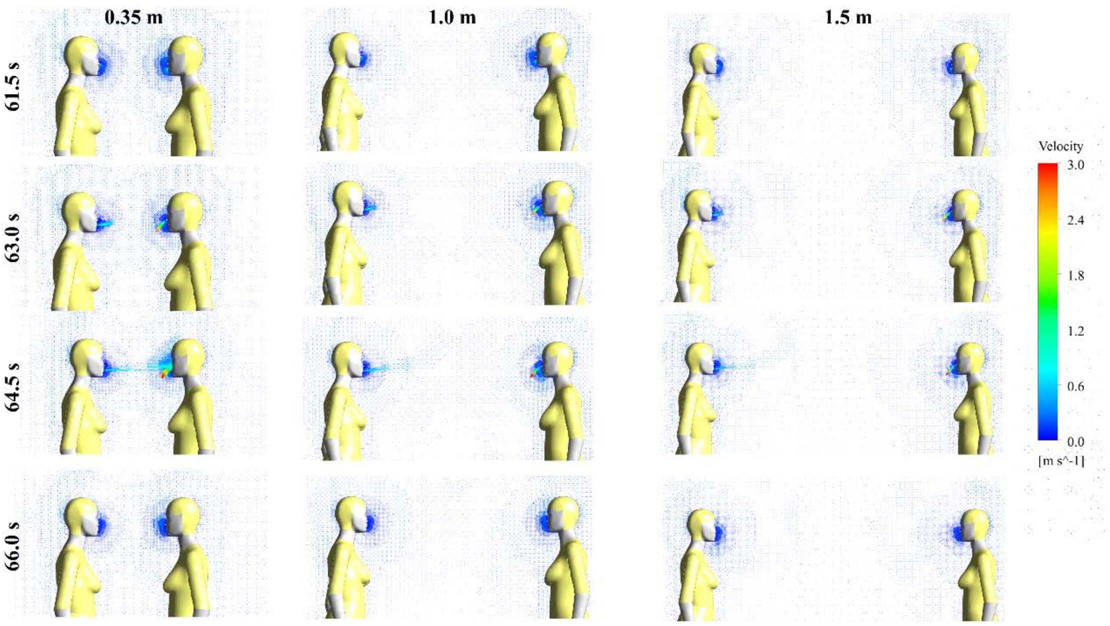

Fig. 4 Velocity distribution in the central plane in the time interval from 60 s to 66 s (10th breathing cycle). The columns refer to the three representative physical distances, namely 0.35 m, 1.0 m, and 1.5 m. The time in different rows refers to the different moments of the breathing phases (Note: the left CTM refers to the infected subject).

Fig. 5 compares the dimensionless mean contaminant concentration (C^+) in the central plane with three representative physical distances. Since airborne contaminants could be transmitted with the airflow, mushroom distribution of the concentration is also observed in the initial stage of the exhalation. Under the dilution effect of the thermal plume and ambient air, the exhaled contaminant gradually begins to diffuse over time. Although the contaminant concentration can be further diluted by the nasal exhalation of the susceptible subject, most of the contaminant still reaches the facial region of the susceptible person at the physical distance of 0.35 m. The distinction between direct and indirect airborne transmission could be determined by the existence of direct contaminant inhalation. Generally, when the infected and the susceptible subjects are in close physical proximity, the exhalation airflow from the infected subject can penetrate the thermal plume and directly enter the facial region of the susceptible one, causing the direct contaminant inhalation [16]. Since the inhaled concentration of the susceptible subject at the large physical distance would share with the background concentration, the direct and indirect airborne transmission could be identified in the range from 1.0 to 1.5 m, which is also reported in previous studies [16, 63]. Considering the impact of the airflow collision on the inhaled contaminant, applying the detailed breathing zone in practice is quite difficult to evaluate human exposure risk. Overall, the present study employs eight monitor points near the mouth and nose of CTMs, and the selection of the monitor points is based on previous studies. The contaminant concentration sampled by the monitor points is compared with the inhalation both in short-term events and under steady-state conditions.

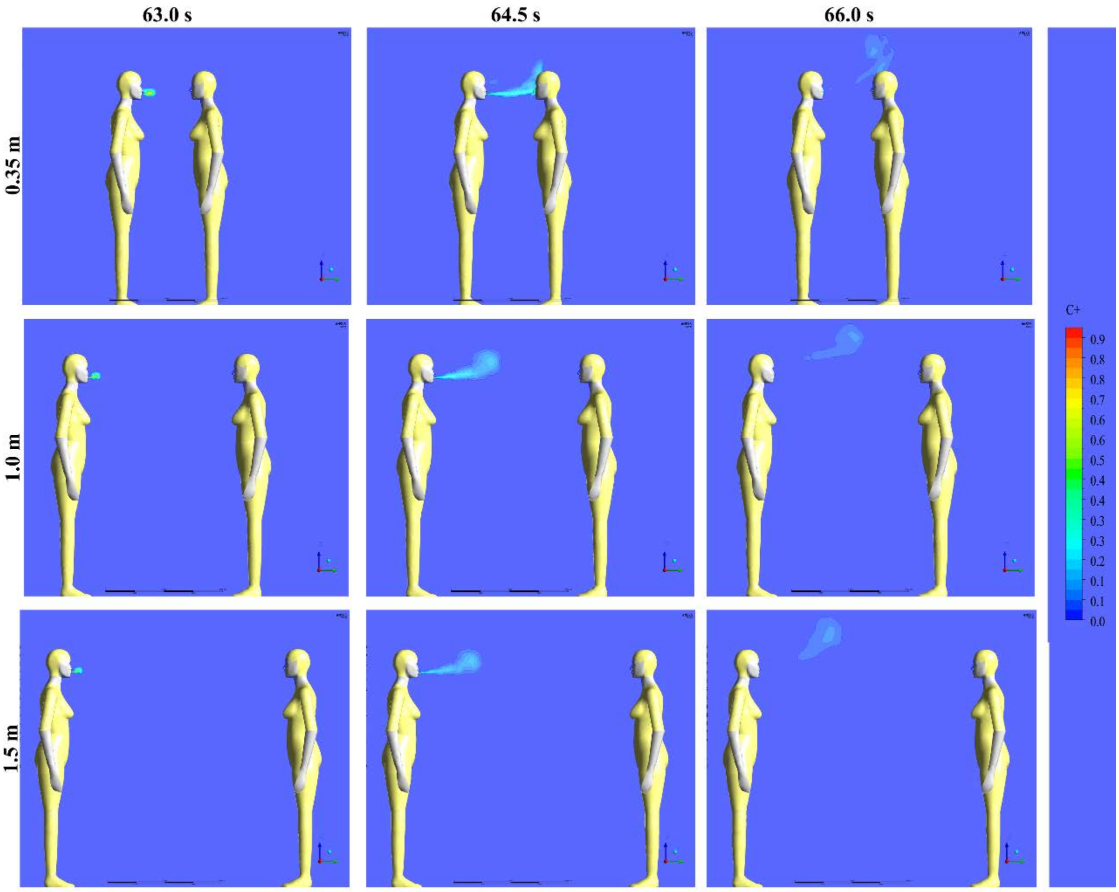

Fig. 5 Distribution of the contaminant concentration (C^+) in different breathing phases with three representative physical distances: 0.35 m, 1.0 m, and 1.5 m (Note: the left CTM refers to the infected subject).

3.3 Exposure risk assessment

The real-time exposure index over time for three physical distances has been presented in Fig. 6, indicating the transient concentration fluctuation. The data is obtained from Point_A since there is no significant difference between Point_A and the inhalation (detailed analysis in Fig. 7 and Fig. 8). The first five minutes of data (gray shadow region) will be discarded from the present study. The averaged (standard deviation) real-time exposure indexes at the physical distance of 0.35 m, 1.0 m, 1.5 m are 1.13

(0.89), 0.96 (0.34), 0.93 (0.30), respectively. The large fluctuation of the real-time exposure index could be attributed to the transient tidal breathing and the airflow interaction in the breathing zone. The fluctuation of the real-time exposure index could also affect the changes in the phase-averaged exposure index. The fluctuation intensity is observed to decrease with the increase of physical distances.

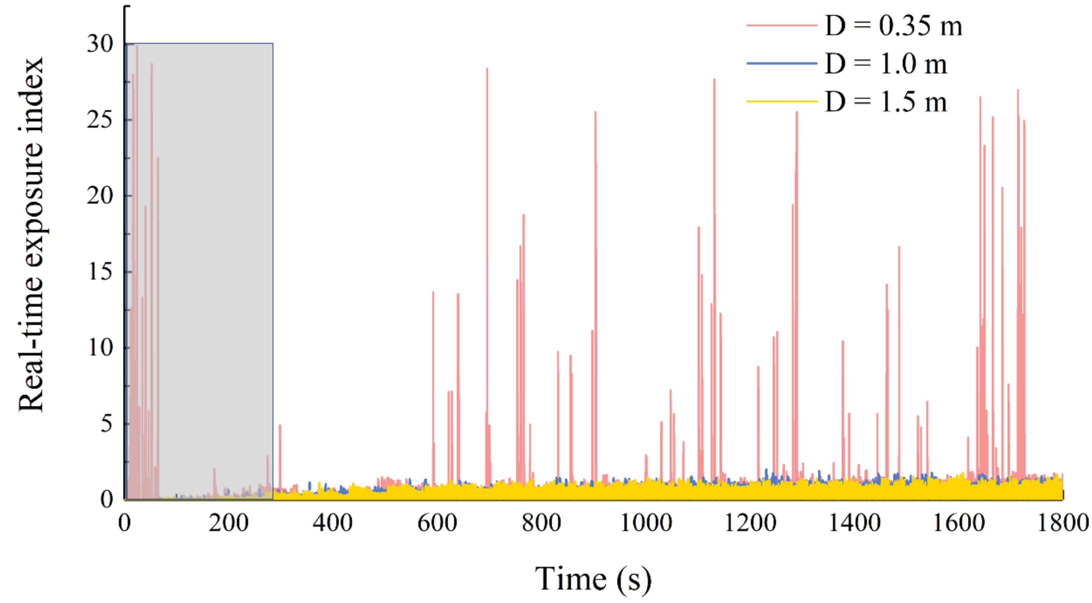

Fig.6 The evolution of real-time exposure index over time at Point_A (discarding the gray shadow region)

Based on concentration data sampled by the eight monitor points and the inhalation, Fig. 7 compares the differences in phase-averaged exposure indexes between various short-term events and steady-state conditions (30 min). The differences in exposure indexes are also observed at three representative physical distances. At the physical distance of 0.35 m (see Fig.7 (a)), the exposure indexes obtained at Point_A and the inhalation are lower than the exposure indexes monitored in the nose tip and upper face (at Point_D, Point_E, and Point_F). The difference is statistically significant ($p < 0.05$). Although there is no statistical difference between the exposure indexes at Point_A, Point_Az, Point_B, Point_C, and the inhalation, further analysis of the turbulence intensity and its concentration fluctuation characteristic will be conducted in the next section. Unlike the condition of 0.35 m, the phase-averaged exposure indexes at the physical distances of 1.0 m and 1.5 m (see Fig. 7 (b) and (c)) are quite similar. Since the airborne contaminant cannot penetrate the thermal plume of the susceptible subjects, the concentration monitored in the eight points is basically related to the background contaminant concentration. Overall, the breathing zone should be identified by comparing the phase-averaged exposure indexes between the monitor points and the inhalation at the physical distance of 0.35 m (the statistical difference, $p < 0.05$). The volume of the breathing zone is in line with the tidal volume (detailed analysis in Section 4). In addition, the phase-averaged exposure indexes obtained at three representative physical distances are observed to maintain the increasing pattern over time. Considering that the first five minutes of data have been discarded from the present study, the aforementioned phenomenon is inconsistent with the previous experimental study [28]. It might be accounted for by the randomness and discreteness characteristics of short-term exposure at the beginning of the event. Therefore, separating the airborne transmission routes and developing the targeted mitigation measures based on their characteristics is critical.

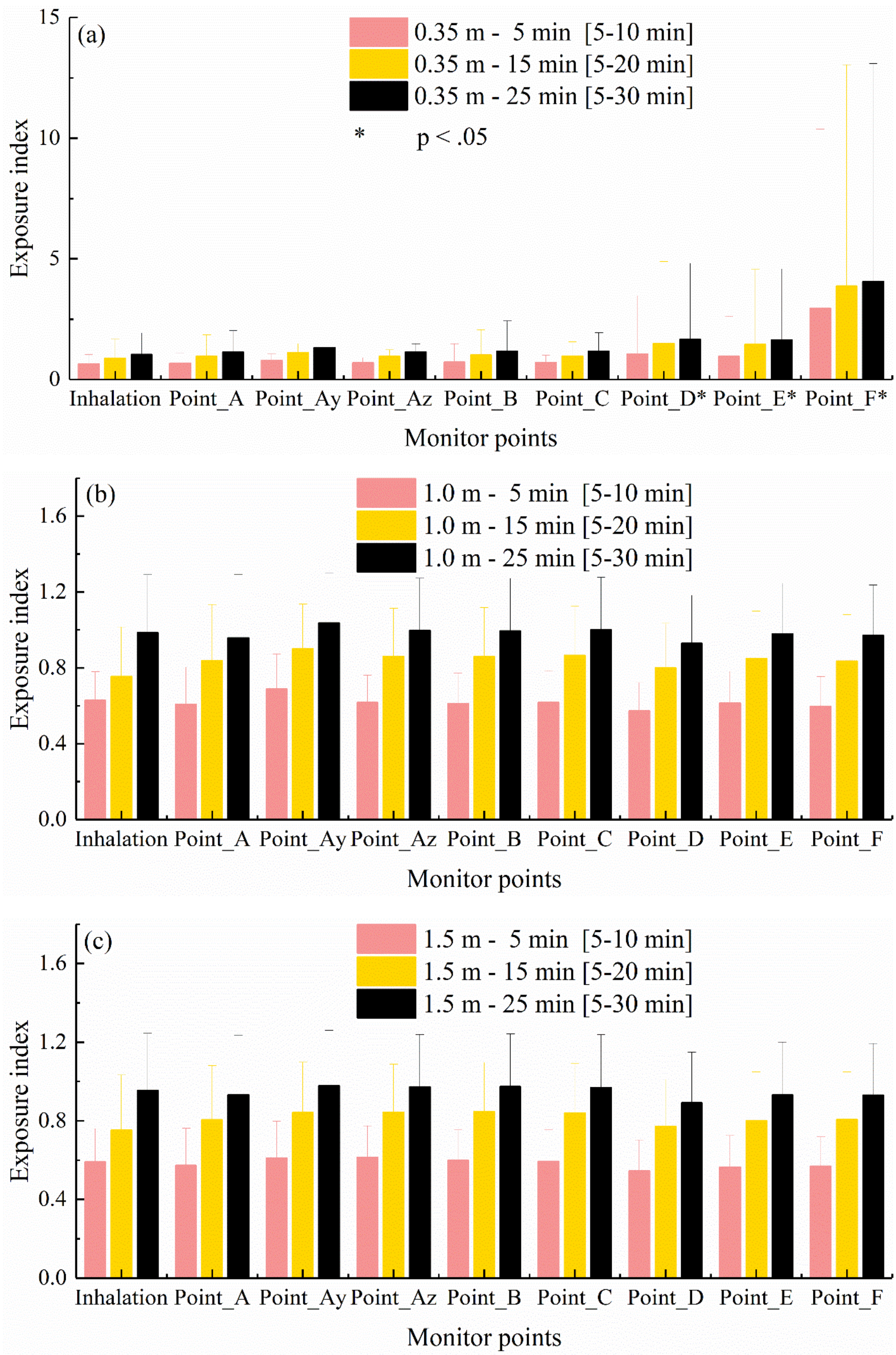

Fig. 7 The exposure indexes from the eight monitor points and the inhalation in various short-term events and steady-state (30 min) conditions: a) 0.35 m; b) 1.0 m; c) 1.5 m.

To compare the phase-averaged exposure indexes between the monitor points and the inhalation, Fig. 8 presents the relative magnitude of their difference at the physical distance of 0.35 m and 1.0 m. The positive value means the exposure index obtained in the monitor point is larger than the inhalation. In Fig. 8 (a), at the physical distance of 0.35 m, Point_Ay, Point_D, Point_E, and Point_F significantly over-estimate the exposure index in comparison with other monitor points. The aforementioned points, located at the nose tip and upper face region, are not recommended for practical measurement. Since the phase-averaged exposure indexes at the distances of 1.0 m and 1.5 m (see Fig. 7 (b) and (c)) are pretty similar, the comparison at the physical distance of 1.0 m is presented in Fig.8 (b). Compared with the distance of 0.35 m, the magnitude of the difference becomes smaller with the increased distance. The exhalation airflow cannot penetrate the micro-environment of the susceptible subject. The little fluctuation might be contributed to the instability of the thermal plume [64]. Overall, if the study only focuses on the time-average concentration field, the contaminant concentration sampled by the four monitor points (Point_A, Point_Az, Point_B, and Point_C) could represent the inhaled concentration of the susceptible subjects. Considering that various infection cases have been reported in short-term events and close physical proximity, it is necessary to analyze the concentration fluctuation characteristics and turbulence intensity of the breathing zone.

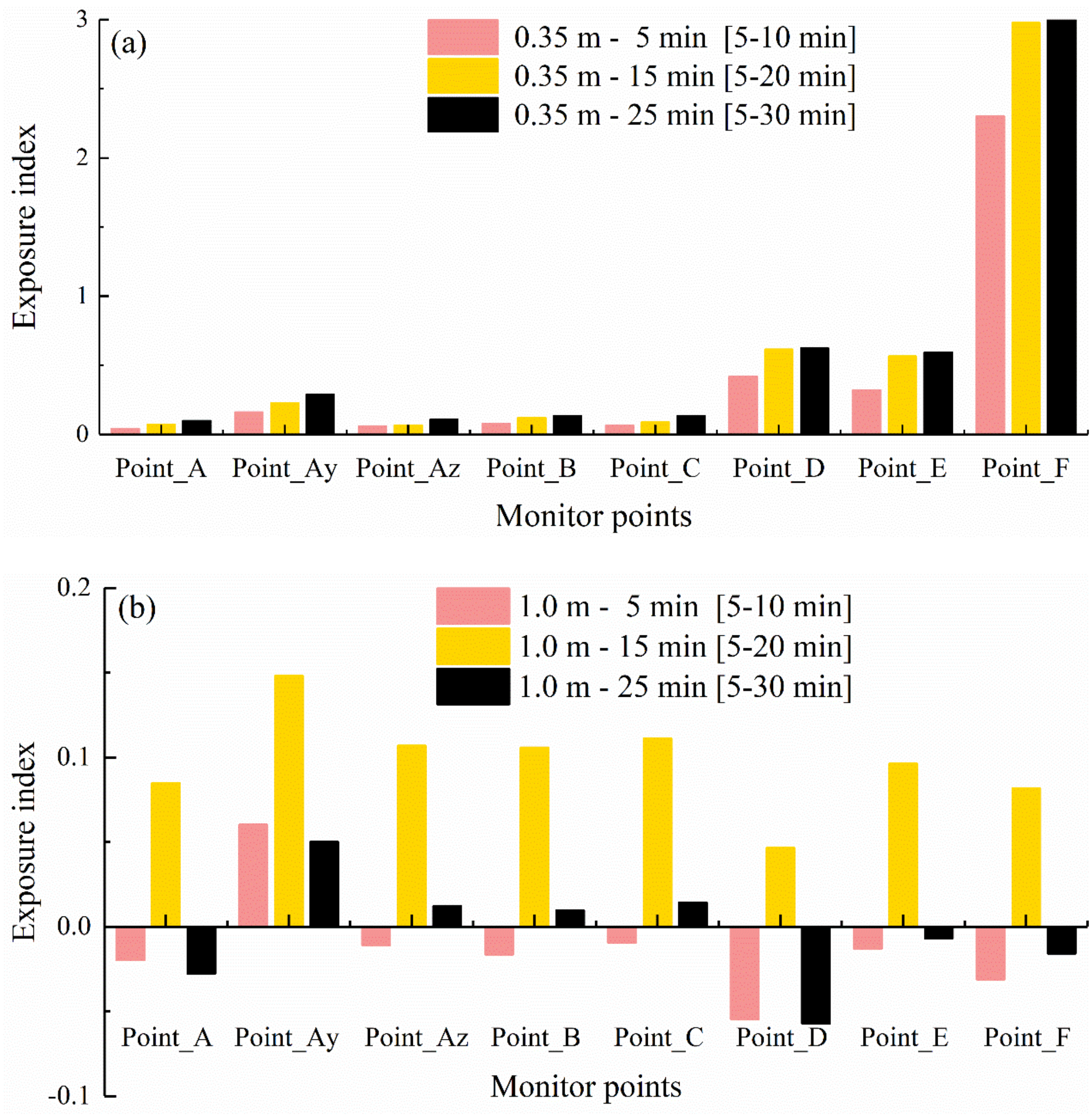

Fig. 8 The relative magnitude of the difference of the exposure indexes between the monitor points and the inhalation, where positive means that the value obtained in the monitor points is larger than the inhalation.

3.4 Turbulence intensity and concentration fluctuation characteristic

Owing to the turbulent nature of the human thermal plume and breathing airflow, the airflow fluctuation could spatially and temporally affect the contaminant distribution no matter whether in short-term events or under steady-state conditions. Notably, short-term events investigated in the study only refer to the building-up background concentration [28]. Compared with previously focused on the steady-state and completely mixing conditions, the formation of the breathing zone should be treated as unsteady in short-term events. Therefore, further analysis of the TI and its concentration fluctuation could provide substantial insight into the breathing zone. The time-averaged TI and phase-averaged TI are employed to indicate the velocity fluctuation characteristics in the monitor points. When calculating the TI, the reference velocity differs among the monitor points, generally in the range of 0.02-0.62 m/s. The largest reference velocity in Point_A is about 0.62 m/s. So, the velocity data in different monitor points are extracted to calculate their turbulence intensity separately.

In Fig. 9, the time-averaged TI and phase-averaged TI of eight monitor points are compared in short-term events (duration of 10 min). Due to periodical breathing, the TI of monitor points in the facial region only changes slightly over different periods. Therefore, the averaged TI is employed to present the comparison. It is observed that the time-averaged TI and phase-averaged TI of eight monitor points are quite distinctive in the facial region. The TI at the nose tip and upper face (like Point_D, Point_E, and Point_F) are generally higher than those near the oral cavity. In Fig. 9 (a), the maximum time-averaged TI even reaches 220% at Point_D (center between the upper lip and nose) in the physical distance of 0.35 m, which could be accounted for by the combined effect of facial features and intense exhalation airflow collision. As for the distance of 1.0 m and 1.5 m, the maximum time-averaged TI in the breathing zone is around 70%. The maximum phase-averaged TI is also found at the Point_D (see Fig. 9 (b)). Nevertheless, the phase-averaged TI is substantially lower than the time-averaged value because the calculation only focuses on the inhalation phase. Given the dynamic breathing conditions, the phase-averaged TI is more suitable for comparison. The phase-averaged TI within the breathing zone is found to be roughly around 40%, which is similar to Cermak et al. [65] - 40%, Xia et al. [66] - 35%. In order to quantify the statistical TI difference between the monitor points, the non-parametric tests (Mann–Whitney U tests) are employed. The statistical difference ($p < 0.05$) between the eight monitor points is observed. Considering the non-homogeneous characteristics of monitor points in the breathing zone, the identified breathing zone by comparing the time-average concentration field is unsuitable for short-term events. Instead of using the identified breathing zone, further evaluating concentration fluctuation characteristics can provide evidence for the appropriate monitor points.

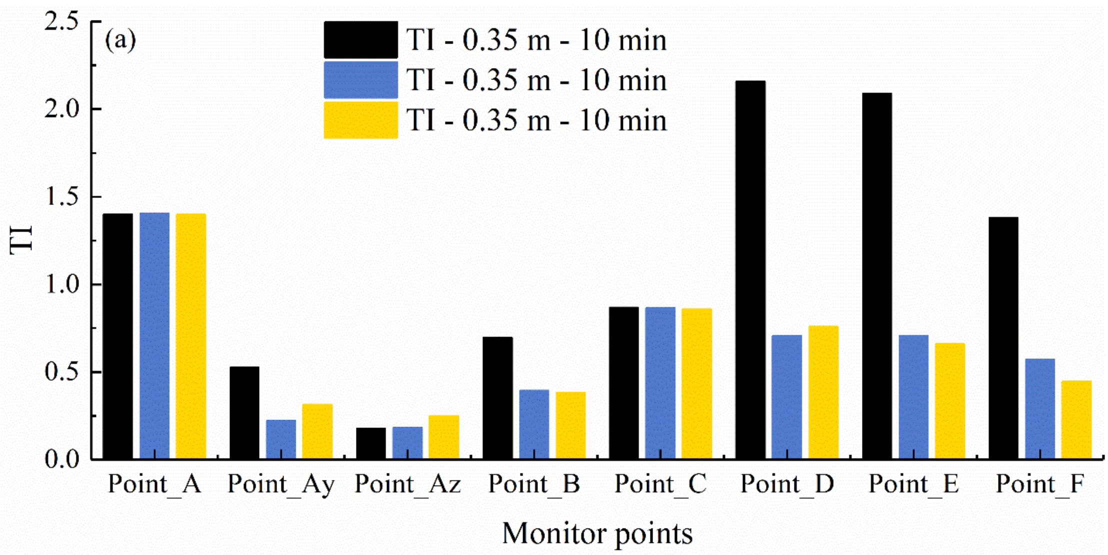

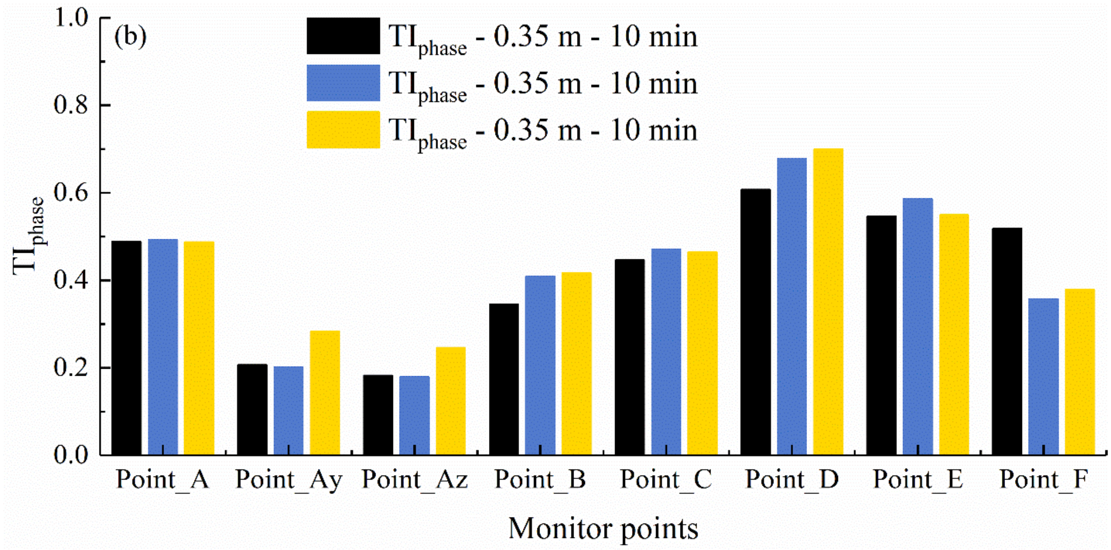

Fig. 9 Time-averaged TI and phase-averaged TI comparison of eight monitor points in short-term events (10 min): a) time-averaged TI; b) phase-averaged TI.

In order to further compare the concentration fluctuation characteristics of the monitor points in the breathing zone, the standard deviation of the phase-averaged exposure indexes is employed. The data shown in Fig. 10 are presented on a logarithmic scale. A large difference in exposure index fluctuation is found between the physical distances of 0.35 m and 1.0/1.5 m. The strong airflow interaction and turbulent nature of the human thermal plume could account for the phenomenon, resulting in a large contaminant fluctuation over time. The contaminant fluctuation depends not only on the turbulence intensity in the breathing zone, but it could also be affected by the turbulent energy distribution among the eddies of different sizes. The Point_Az is especially unsuitable for the instant exposure risk analysis since it cannot reflect the contaminant fluctuation characteristics in the facial region. Overall, the analysis of instant exposure risk in short-term events should consider its turbulence intensity and concentration fluctuation characteristic. Point_A, Point_B, and Point_C can be employed as the appropriate monitor points to evaluate the instant infection risk in short-term events. Due to the large temporal variation of the contaminant concentration in the identified breathing zone, short-term airborne transmission events are quite possible to occur within short physical distances. The development of targeted mitigation measures is critical.

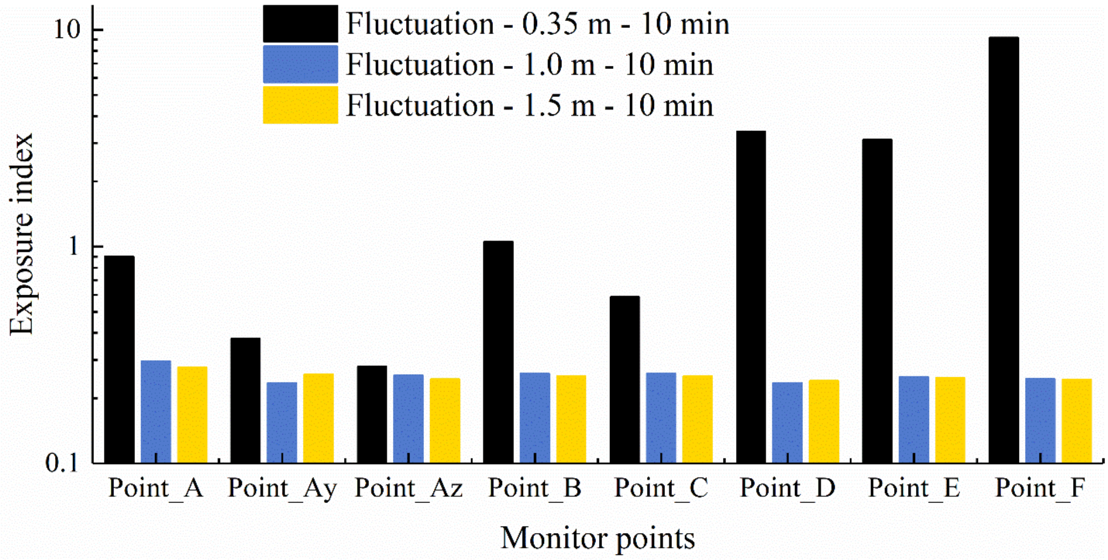

Fig. 10 Concentration fluctuation of eight monitor points in 10-min short-term events (represented by exposure index).

4 Discussion

Depending on the background concentration and physical distances, airborne transmission can be divided into two categories and four combinations, namely, a) building-up background concentration: short and long physical distance; b) steady-state background concentration: short and long physical distance. Notably, plenty of previous studies focused on steady-state exposure, but few studied short-term exposure events [67]. The present study is restricted to the scenarios with building-up one, where the infected subject has just entered the space. When two subjects are in close proximity, such as in the consultation of physicians, short meetings, offices, canteens, etc., the formation of the breathing zone should be treated as unsteady in short-term events. The widely employed monitor points in the facial region could not be representative to indicate the inhaled concentration. With the increase in physical distance, the indoor ventilation airflow could affect the cross-transmission risk. The distance of 1.0 m and 1.5 m, acting as the threshold distance for the direct and indirect airborne transmission [16], can also be employed to determine the formation characteristics of the breathing zone. Overall, if the domain airflow is the respiratory airflow (less than 1.0 m in the present study), the formation of the breathing zone should be treated as unsteady. In addition, the present study focuses on the scenarios of building-up background concentration. Before reaching the steady-state, the infection events should be treated as short-term events, and the unsteady nature of the breathing zone should be considered. The steady-state condition in short-term events refers to when the averaged airspeed and contaminant concentration in the ventilation exhaust reaches relatively stable [28].

Overall, if the study only focuses on the time-average concentration field, the breathing zone could be treated as steadily formed. That is because the timescale of breathing is much smaller than that of room ventilation. The performance of the eight widely employed monitor points has been evaluated compared with the inhalation by the phase-averaged exposure indexes (in Fig. 7 and Fig. 8). At the physical distance of 0.35 m, the Point_Ay, Point_D, Point_E, and Point_F significantly over-estimate the exposure indexes. The aforementioned points are not recommended in the practical measurement. Previous studies treated the Point_E, at the nose tip, as the optimal location [23, 45]. However, the present study quantitatively observed a significant difference compared with inhalation. Besides, Point_D, at the center between the upper lip and nose, has been proved in ordinary performance due to facial features' effect on contaminant distribution. The obtained results were in line with a recent experimental study [5]. The contaminant concentration sampled by the other four monitor points (Point_A, Point_Az, Point_B, and Point_C) in the identified breathing zone could represent the inhaled concentration of the susceptible subjects.

In comparison, if the study focuses on short-term events, the formation of the breathing zone is not steady. The instant exposure risk assessment should consider the turbulence intensity and concentration fluctuation characteristics (in Fig. 9 and Fig. 10), especially considering the randomness and discreteness characteristics of short-term events [68]. In addition, the Point_Az is especially not suitable for the instant exposure risk analysis since it cannot reflect the contaminant fluctuation characteristics in the facial region. Therefore, the identified breathing zone proposed by comparing the time-average concentration field is not applicable for short-term events, along with the over-and under-estimation. Instead of using the identified breathing zone, Point_A, Point_B, and

Point_C can be employed as the appropriate monitor points to evaluate the infection risk in short-term events. Fig. 11 presents the identified breathing zone in mixing ventilation under different conditions: steady-formation and unsteady-formation in short-term events. In Fig.11 (a), the volume of recommended sampling region is in line with the tidal volume. If the study only focuses on the time-average concentration field, the contaminant monitored at the sampling points in the box is approximately in line with the contaminant inhaled by the infected person. The suggested breathing zone is similar to a recent study using the reversed time-traced virtual flow field and the scale for ventilation efficiency 5 (SVE 5) [4]. The slight discrepancy in the breathing zone dimension could be accounted for by the difference in the breathing pattern and tidal volume. For short-term events, the formation of the breathing zone could be treated as unsteady. Instead of using the identified breathing zone, Point_A (located at the center of the lips), Point_B (located at the left corner of the mouth), and Point_C (located at the center between the chin and lower lip) perform well in capturing the fluctuation characteristics of short-term events [69, 70]. Considering the difficulty of performing the measurement at the three aforementioned points, the air sampling tube attached to the headset and even glasses have been designed for accurate measurement [5, 45].

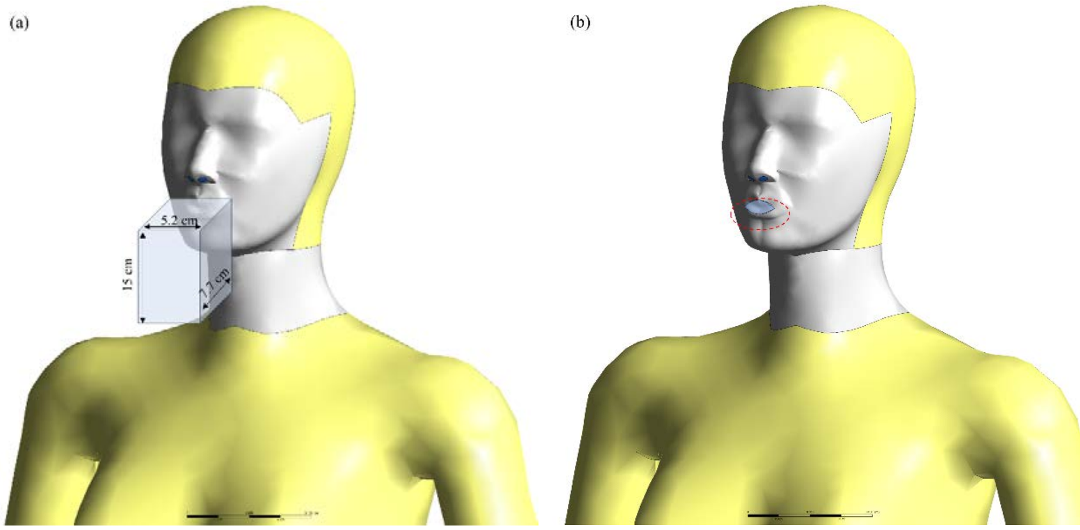

Fig. 11 Identified breathing zone in mixing ventilation under different conditions: (a) steady-formation; (b) unsteady-formation in short-term events.

Owing to the instantaneous and tidal properties of the respiratory airflow, it gradually becomes fully turbulent and further mixes with the ambient ventilation airflow with development. The interaction between the respiratory, ventilation airflow, and the thermal plume rising from the heated human body significantly affect the turbulence intensity and concentration fluctuation in the facial region of the susceptible subjects. Although the known instant exposure risk may be caused by tidal breathing, to the best of our knowledge, there is no study to distinguish the difference between the concentration distribution in the facial region and inhalation in short-term events. The observed randomness and discreteness characteristics of the short-term events highlight the necessity of developing the targeted precautionary measures. When two subjects are in close physical proximity, increasing the room ventilation rate may have a moderate or limited impact on short-term events [67, 68]. Although the room ventilation can help dilute and reduce the background concentration, the background value in the present study (building-up scenario) is relatively lower than that in the steady-state scenario. Therefore, engineering control measures like the localized ventilation/exhaust system, air purifiers, and physical barriers should be highly recommended [71, 72]. Maintaining physical distancing and wearing surgical masks still act as the best protection against the Delta and Omicron variants [73].

5 Limitation and future work

The general requirement of the LES is to determine the allowable cell size to resolve at least 80% turbulent kinetic energy [74]. Owing to the difficulty of obtaining the complete energy spectrum, the Length Scale Resolution (LSR) has been adopted as a metric to present the mesh resolution [75]. $LSR = \bar{\Delta}/l_{DI}$ where the l_{DI} is the lower limit of the inertial sub-range. The average LSR in the present study is 6.21, slightly exceeding the upper limit value (5.0). Considering that the global quality of the simulation cannot be estimated by the LSR metrics only, it should also be evaluated from the match between the simulation and experiments [76]. The study is limited without considering the humidity of the exhaled airflow, while the exhaled airflow humidity might impact the breathing zone at different humidity levels. Special scenarios like dental surgery environment [77, 78] and gym [79] should be further studied. The present study has validated the thermal plume around the human body. A future experimental study should be conducted to monitor the exhaled contaminant dispersion in other room points and thus act as supplementary validation data. Additionally, the breathing pattern and the phase difference between two breathings might also affect the scale of the breathing zone. Since human subjects can unconsciously change their breathing mode, breathing in the same mode is quite challenging. Thus, examining the identified breathing zone in different breathing combinations is necessary. Since the room occupants could move around, the breathing zone could be considerably impacted by the change of thermal plume. Therefore, further investigation into the breathing zone should be conducted.

6 Conclusions

The present study quantitatively assesses the eight commonly-used inhalation monitor points in the facial region by recording the contaminant distribution and fluctuation characteristics under steady-state conditions and short-term events. The results could help to select the proper monitor points under different conditions and further develop the targeted precautionary measures:

1) Based on the statistical difference in the contaminant distribution at the short physical distance (0.35 m), the breathing zone could be identified from the time-averaged concentration field.
2) The identified breathing zone proposed by comparing the time-average concentration field is not applicable for short-term events. Point_E, at the nose tip, is not the optimal location to represent the inhaled concentration. In comparison, Point_A (located at the center of the lips), Point_B (located at the left corner of the mouth), and Point_C (located at the center between the chin and lower lip) perform much better in short-term events. Wearable devices for accurate measurement

should be developed.

3) Due to the substantial temporal variation of the contaminant in the identified breathing zone, the analysis of instant exposure risk in short-term events should consider its turbulence intensity and concentration fluctuation characteristic. The localized method with direct interference on the respiratory airflow should be recommended in short-term events.

Acknowledgments

This study was supported by the Ph.D. studentship funded by the Hong Kong Polytechnic University and partially supported by the National Natural Science Foundation of China (No. 51908203) and the Fundamental Research Funds for the Central Universities (No. 531118010378). The authors thank Miss Zenan Xian for her help in the pre-project work.

Declaration of competing interest

The authors declare that they have no known competing financial interests or personal relationships that could have appeared to influence the work reported in this paper.

Reference

1. WHO. *COVID-19 Weekly Epidemiological Update*. 2022; Available from: https://www.who.int/publications/m/item/weekly-epidemiological-update-on-covid-19---5-april-2022.
2. Li, X., et al., *Restoration of dental services after COVID-19: The fallow time determination with laser light scattering.* Sustainable Cities and Society, 2021. **74**: p. 103134.
3. Xu, C., et al., *Prediction and control of aerosol transmission of SARS-CoV-2 in ventilated*

context: from source to receptor. Sustainable cities and society, 2022. **76**: p. 103416.

4. Kuga, K., P. Wargocki, and K. Ito, *Breathing zone and exhaled air re-inhalation rate under transient conditions assessed with a computer-simulated person.* Indoor air, 2022. **32**(2): p. e13003.
5. Kierat, W., et al., *Towards enabling accurate measurements of CO2 exposure indoors.* Building and Environment, 2022. **213**: p. 108883.
6. Liu, L., et al., *Evaporation and dispersion of respiratory droplets from coughing.* Indoor air, 2017. **27**(1): p. 179-190.
7. Li, Y., et al., *Probable airborne transmission of SARS-CoV-2 in a poorly ventilated restaurant.* Building and Environment, 2021. **196**: p. 107788.
8. Van Doremalen, N., et al., *Aerosol and surface stability of SARS-CoV-2 as compared with SARS-CoV-1.* New England journal of medicine, 2020. **382**(16): p. 1564-1567.
9. Chen, W., et al., *Extended short-range airborne transmission of respiratory infections.* Journal of hazardous materials, 2022. **422**: p. 126837.
10. Balachandar, S., et al., *Host-to-host airborne transmission as a multiphase flow problem for science-based social distance guidelines.* International Journal of Multiphase Flow, 2020. **132**: p. 103439.
11. Sarhan, A., P. Naser, and J. Naser, *COVID-19 aerodynamic evaluation of social distancing in indoor environments, a numerical study.* Journal of Environmental Health Science and Engineering, 2021. **19**(2): p. 1969-1978.
12. Issakhov, A., et al., *A numerical assessment of social distancing of preventing airborne transmission of COVID-19 during different breathing and coughing processes.* Scientific Reports, 2021. **11**(1): p. 1-39.
13. Cao, G., et al., *Protected zone ventilation and reduced personal exposure to airborne cross-infection.* Indoor Air, 2015. **25**(3): p. 307-319.
14. Arumuru, V., J. Pasa, and S.S. Samantaray, *Experimental visualization of sneezing and efficacy of face masks and shields.* Physics of Fluids, 2020. **32**(11): p. 115129.
15. Ai, Z., T. Huang, and A. Melikov, *Airborne transmission of exhaled droplet nuclei between occupants in a room with horizontal air distribution.* Building and Environment, 2019. **163**: p. 106328.
16. Liu, L., et al., *Short-range airborne transmission of expiratory droplets between two people.* Indoor air, 2017. **27**(2): p. 452-462.
17. CDC. *Centers for Disease Control and Prevention (CDC) About COVID-19*. 2022; Available from: https://www.cdc.gov/.
18. Feng, Y., et al., *Influence of wind and relative humidity on the social distancing effectiveness to prevent COVID-19 airborne transmission: A numerical study.* Journal of aerosol science, 2020. **147**: p. 105585.
19. Sun, C. and Z. Zhai, *The efficacy of social distance and ventilation effectiveness in preventing COVID-19 transmission.* Sustainable cities and society, 2020. **62**: p. 102390.
20. Setti, L., et al., *Airborne transmission route of COVID-19: Why 2 meters/6 feet of inter-personal distance could not be enough*. 2020, Multidisciplinary Digital Publishing Institute. p. 2932.
21. Lidén, G. and J. Waher, *Experimental investigation of the concept of a 'breathing zone'using a mannequin exposed to a point source of inertial/sedimenting particles emitted with momentum.* Annals of occupational hygiene, 2010. **54**(1): p. 100-116.

22. Al Assaad, D., S. Yang, and D. Licina, *Particle release and transport from human skin and clothing: A CFD modeling methodology.* Indoor air, 2021. **31**(5): p. 1377-1390.
23. Geiss, O., *Effect of wearing face masks on the carbon dioxide concentration in the breathing zone.* Aerosol and Air Quality Research, 2021. **21**(2): p. 200403.
24. Rim, D. and A. Novoselac, *Transport of particulate and gaseous pollutants in the vicinity of a human body.* Building and Environment, 2009. **44**(9): p. 1840-1849.
25. Yan, Y., et al., *Evaluation of airborne disease infection risks in an airliner cabin using the Lagrangian-based Wells-Riley approach.* Building and Environment, 2017. **121**: p. 79-92.
26. You, R., et al., *Evaluating the commercial airliner cabin environment with different air distribution systems.* Indoor Air, 2019. **29**(5): p. 840-853.
27. Gupta, J., C.H. Lin, and Q. Chen, *Inhalation of expiratory droplets in aircraft cabins.* Indoor Air, 2011. **21**(4): p. 341-350.
28. Ai, Z., K. Hashimoto, and A.K. Melikov, *Airborne transmission between room occupants during short-term events: Measurement and evaluation.* Indoor air, 2019. **29**(4): p. 563-576.
29. Anthony, T.R., M.R. Flynn, and A. Eisner, *Evaluation of facial features on particle inhalation.* Annals of Occupational Hygiene, 2005. **49**(2): p. 179-193.
30. Li, X., Y. Yan, and J. Tu, *The simplification of computer simulated persons (CSPs) in CFD models of occupied indoor spaces.* Building and Environment, 2015. **93**: p. 155-164.
31. Yan, Y., et al., *Evaluation of manikin simplification methods for CFD simulations in occupied indoor environments.* Energy and Buildings, 2016. **127**: p. 611-626.
32. Faleiros, D.E., et al., *TU Delft COVID-app: A tool to democratize CFD simulations for SARS-CoV-2 infection risk analysis.* Science of the Total Environment, 2022: p. 154143.
33. Naseri, A., O. Abouali, and G. Ahmadi, *Effect of turbulent thermal plume on aspiration efficiency of micro-particles.* Building and Environment, 2017. **118**: p. 159-172.
34. Zhu, S., et al., *Study on inhalation region by means of CFD analysis and experiment.* Building and Environment, 2005. **40**(10): p. 1329-1336.
35. Villafruela, J., I. Olmedo, and J. San José, *Influence of human breathing modes on airborne cross infection risk.* Building and Environment, 2016. **106**: p. 340-351.
36. Wu, J. and W. Weng, *COVID-19 virus released from larynx might cause a higher exposure dose in indoor environment.* Environmental Research, 2021. **199**: p. 111361.
37. Times, K. *Delta variant can infect a person within 15 seconds as Cambodia logs 75 total cases of COVID-19 Delta infections*. 2021; Available from: https://www.khmertimeskh.com/50895595/delta-variant-can-infect-a-person-within-15-seconds-as-cambodia-logs-75-cases-of-covid-19-delta-infections/.
38. Kongnov, T. *Delta can spread in 15 seconds*. 2021; Available from: https://www.khmertimeskh.com/50902050/delta-can-spread-in-15-seconds.
39. Bhattacharyya, S., et al., *A novel CFD analysis to minimize the spread of COVID-19 virus in hospital isolation room.* Chaos, Solitons & Fractals, 2020. **139**: p. 110294.
40. Hang, J., et al., *Potential airborne transmission between two isolation cubicles through a shared anteroom.* Building and Environment, 2015. **89**: p. 264-278.
41. Zhang, Z., et al., *Disease transmission through expiratory aerosols on an urban bus.* Physics of Fluids, 2021. **33**(1): p. 015116.
42. Ai, Z., C.M. Mak, and J. Niu, *Numerical investigation of wind-induced airflow and interunit dispersion characteristics in multistory residential buildings.* Indoor air, 2013. **23**(5): p. 417-

429.

43. Ai, Z. and C.M. Mak, *A study of interunit dispersion around multistory buildings with single-sided ventilation under different wind directions.* Atmospheric Environment, 2014. **88**: p. 1-13.

44. Ai, Z., K. Hashimoto, and A.K. Melikov, *Influence of pulmonary ventilation rate and breathing cycle period on the risk of cross-infection.* Indoor Air, 2019. **29**(6): p. 993-1004.

45. Pantelic, J., et al., *Personal CO2 cloud: laboratory measurements of metabolic CO2 inhalation zone concentration and dispersion in a typical office desk setting.* Journal of exposure science & environmental epidemiology, 2020. **30**(2): p. 328-337.

46. Melikov, A., *Breathing thermal manikins for indoor environment assessment: important characteristics and requirements.* European journal of applied physiology, 2004. **92**(6): p. 710-713.

47. Xu, C., et al., *Human exhalation characterization with the aid of schlieren imaging technique.* Building and environment, 2017. **112**: p. 190-199.

48. Bolashikov, Z.D., M. Barova, and A.K. Melikov, *Wearable personal exhaust ventilation: Improved indoor air quality and reduced exposure to air exhaled from a sick doctor.* Science and Technology for the Built Environment, 2015. **21**(8): p. 1117-1125.

49. Yang, J., et al., *A time-based analysis of the personalized exhaust system for airborne infection control in healthcare settings.* Science and Technology for the Built Environment, 2015. **21**(2): p. 172-178.

50. Villafruela, J., et al., *CFD analysis of the human exhalation flow using different boundary conditions and ventilation strategies.* Building and Environment, 2013. **62**: p. 191-200.

51. Bazdidi-Tehrani, F., et al. *Large eddy simulation of pollutant dispersion in a naturally cross-ventilated model building: Comparison between sub-grid scale models*. in *Building Simulation*. 2019. Springer.

52. Dai, Y., et al., *Evaluation of computational and physical parameters influencing CFD simulations of pollutant dispersion in building arrays.* Building and Environment, 2018. **137**: p. 90-107.

53. Ai, Z. and C.M. Mak, *Large-eddy Simulation of flow and dispersion around an isolated building: analysis of influencing factors.* Computers & Fluids, 2015. **118**: p. 89-100.

54. Du, Y., et al., *Efficient and high-resolution simulation of pollutant dispersion in complex urban environments by island-based recurrence CFD.* Environmental Modelling & Software, 2021. **145**: p. 105172.

55. Deng, Z. and Q. Chen, *What is suitable social distancing for people wearing face masks during the COVID-19 pandemic?* Indoor air, 2022. **32**(1): p. e12935.

56. Liu, W., et al., *Exploring the potentials of personalized ventilation in mitigating airborne infection risk for two closely ranged occupants with different risk assessment models.* Energy and Buildings, 2021. **253**: p. 111531.

57. Melikov, A.K. and V. Dzhartov, *Advanced air distribution for minimizing airborne cross-infection in aircraft cabins.* Hvac&R Research, 2013. **19**(8): p. 926-933.

58. Licina, D., et al., *Experimental investigation of the human convective boundary layer in a quiescent indoor environment.* Building and Environment, 2014. **75**: p. 79-91.

59. Adrian, R.J. and J. Westerweel, *Particle image velocimetry*. 2011: Cambridge university press.

60. Schatzmann, M., *COST 732 model evaluation case studies: approach and results*. 2010: Meteorological Inst.

61. Arpino, F., et al., *A Eulerian-Lagrangian approach for the non-isothermal and transient CFD analysis of the aerosol airborne dispersion in a car cabin.* Building and Environment, 2022. **209**: p. 108648.
62. Jiang, N., et al., *Experimental study on flow behavior of breathing activity produced by a thermal manikin.* Building and Environment, 2017. **123**: p. 200-210.
63. Liu, F., et al., *Direct or indirect exposure of exhaled contaminants in stratified environments using an integral model of an expiratory jet.* Indoor Air, 2019. **29**(4): p. 591-603.
64. Zong, J., et al., *A review of human thermal plume and its influence on the inhalation exposure to particulate matter.* Indoor and Built Environment, 2022: p. 1420326X221080358.
65. Cermak, R., et al. *PIV measurements at the breathing zone with personalized ventilation*. in *Proceedings of the Eight International Conference Air Distribution in Rooms, Roomvent, Copenhagen, Denmark*. 2002.
66. Xia, Y., et al., *Effects of turbulent air on human thermal sensations in a warm isothermal environment.* Indoor air, 2000. **10**(4): p. 289-296.
67. Ai, Z.T. and A.K. Melikov, *Airborne spread of expiratory droplet nuclei between the occupants of indoor environments: A review.* Indoor air, 2018. **28**(4): p. 500-524.
68. Li, X., et al. *Airborne transmission during short-term events: Direct route over indirect route*. in *Building Simulation*. 2022. Springer.
69. Bivolarova, M., et al., *Effect of airflow interaction in the breathing zone on exposure to bio-effluents.* Building and Environment, 2017. **125**: p. 216-226.
70. Melikov, A. and J. Kaczmarczyk, *Measurement and prediction of indoor air quality using a breathing thermal manikin.* Indoor air, 2007. **17**(1): p. 50-59.
71. Ye, J., Z. Ai, and C. Zhang, *A new possible route of airborne transmission caused by the use of a physical partition.* Journal of Building Engineering, 2021. **44**: p. 103420.
72. Xu, C., et al., *Effects of personalized ventilation interventions on airborne infection risk and transmission between occupants.* Building and Environment, 2020. **180**: p. 107008.
73. Eikenberry, S.E., et al., *To mask or not to mask: Modeling the potential for face mask use by the general public to curtail the COVID-19 pandemic.* Infectious disease modelling, 2020. **5**: p. 293-308.
74. Pope, S.B., *Ten questions concerning the large-eddy simulation of turbulent flows.* New journal of Physics, 2004. **6**(1): p. 35.
75. Brusiani, F., C. Forte, and G.M. Bianchi, *Assessment of a numerical methodology for large eddy simulation of ice wall bounded non-reactive flows*. 2007, SAE Technical Paper.
76. Piscaglia, F., et al., *Boundary conditions and sgs models for les of wall-bounded separated flows: An application to engine-like geometries.* Oil & Gas Science and Technology–Revue d'IFP Energies nouvelles, 2014. **69**(1): p. 11-27.
77. Li, X., et al., *Evaluating flow-field and expelled droplets in the mockup dental clinic during the COVID-19 pandemic.* Physics of Fluids, 2021. **33**(4): p. 047111.
78. Li, X., et al., *How the high-volume evacuation alters the flow-field and particle removal characteristics in the mock-up dental clinic.* Building and Environment, 2021. **205**: p. 108225.
79. Blocken, B., et al., *Ventilation and air cleaning to limit aerosol particle concentrations in a gym during the COVID-19 pandemic*. Building and Environment, 2021. **193**: p. 107659.